ARCHIVES OF ELECTRICAL ENGINEERING VOL. 62(1), pp. 111-122 (2013)

DOI 10.2478/aee-2013-0008

Analysis of the electromagnetic response of complex dispersive material with the single-step wideband finite element method

BOGUSŁAW BUTRYŁO

Białystok Technical University
Faculty of Electrical Engineering
ul. Wiejska 45D, 15-351 Białystok, Poland
e-mail: b.butrylo@pb.edu.pl

(Received: 19.05.2012, revised: 12.11.2012)

Abstract: The paper describes the formulation and implementation of the broadband finite element time domain algorithm. The presented formalism is valid to analysis of electromagnetic phenomena in linear, frequency selective materials. The complex profile of permittivity of materials is approximated using a set of the Lorentz resonance models. The solution of the integro-differential second order equation is obtained using a single-step integration scheme and a recursive convolution algorithm. The discussed formulation enables to adopt the structure of the narrowband part as well as the phase of calculation of the convolution equations for the subsequent components. The properties of the algorithm are validated using a finite difference broadband algorithm.

Key words: propagation of electromagnetic pulse, dielectric dispersion, frequency selective materials, broadband time-domain simulation, finite element time-domain method

1. Introduction

The development of high frequency equipment is inherently coupled with implementation of some new, hybrid materials [7, 12, 16]. The discussed set of materials consists of at least two quite different groups, with disordered internal structure and with periodic, totally ordered structure. Some compounds, polymers and mixtures, as well as Marconi materials, constitute the first group. The second one covers some layered materials and electric metamaterials. In the context of high frequency applications, these materials show some interesting features. Their electric properties are frequency dependent and they can be adjusted to the desired form by modification of the internal structure. The rate of selected inclusions and their arrangement in a microscopic scale bring on modification of the local electromagnetic field. In that way, the damping and transmission coefficients of these materials can be fitted in the assumed frequency band.

Numerical analysis of electromagnetic fields in frequency-dependent materials requires implementation of a time-domain algorithm. Direct integration of Maxwell equations arises due to required estimation of some polarization phenomena. The typical solution of this problem is based on a leap-frog finite difference time-domain algorithm [5, 15]. Some wideband formulation of the finite element algorithm is delivered in [4, 8, 9].

The paper deals with a broadband single-step formulation of the finite element (FE) algorithm. The constitutive equation is split into a set of self-dependent ordinary differential equations and integral equations. The convolution part of the equation is calculated using a recursive scheme. The structure of the single-step scheme, based on a systematic decomposition into the narrowband part and the phase of calculation of polarization, is presented and discussed. The proposed structural coupling between these parts enables one to implement different algorithmic solutions of the subroutines. Validation of the presented finite element algorithm has been performed by considering a three-dimensional benchmark problem.

2. Material properties

Macroscopic analysis of electromagnetic phenomena requires an instantaneous representation of the electric parameters. According to linear properties of the analyzed materials, the complex, frequency-dependent profile of permittivity $\underline{\varepsilon}_r(\omega) = \varepsilon_r'(\omega) - j\varepsilon_r''(\omega)$ can be expressed as a sum of a real value optical dielectric constant ε_∞ and a complex function of susceptibility $\underline{\chi}(\omega)$ [6]

$$\underline{\varepsilon}_r(\omega) = \varepsilon_\infty + \underline{\chi}(\omega). \tag{1}$$

For the assumed frequency span up to 1-10 GHz, the permeability of materials remains constant ($\mu_r = 1$). In the analyzed dielectric structures, any conduction currents are neglected ($\sigma = 0$).

Any real profile of susceptibility of linear material can be approximated using an additive form of the constructed model

$$\underline{\chi}(\omega) \xrightarrow{approximation} \underline{\chi}_A(\omega).$$

In this approach, the frequency variation of susceptibility is expressed by a set of Lorentz submodels [5, 6]

$$\underline{\chi}_A(\omega) = \sum_{n=1}^{N} \underline{\chi}_n(\omega) = \sum_{n=1}^{N} \frac{\Delta_{\varepsilon,n}\omega_{0,n}^2}{\omega_{0,n}^2 + 2j\omega\nu_n - \omega^2}, \tag{2}$$

where $\Delta_{\varepsilon,n}$ is the decrement of permittivity of the n-th component. The banded properties of the constructed model are changed by modification of the number of submodels N and their parameters. Since the resonant angular frequency $\omega_{0,n}$ of any submodel is larger than the suitable damping coefficient ν_n, each component behaves as a narrowband oscillator. In that case the counterpart form of the Equation (2) can be written as

$$\chi_n(t) = \frac{\Delta_{\varepsilon,n}\omega_{0,n}^2}{\sqrt{\omega_{0,n}^2 - \nu_n^2}} \sin\left(\sqrt{\omega_{0,n}^2 - \nu_n^2}\, t\right) \mathrm{e}^{-\nu_n t}\, \mathbf{1}(t), \tag{3}$$

where $\mathbf{1}(t)$ is the unit step function. Taking into account the simplicity of the later form of the algorithm, the typical time-domain form of the Lorentz oscillator (3) is replaced using an exponential kernel

$$\underline{\chi}_n(t) = -j \frac{\Delta_{\varepsilon,n}\omega_{0,n}^2}{\sqrt{\omega_{0,n}^2 - \nu_n^2}} \mathrm{e}^{-\left(\nu_n - j\sqrt{\omega_{0,n}^2 - \nu_n^2}\right)t} \mathbf{1}(t). \tag{4}$$

Returning to the basic form of the susceptibility function requires calculation of the real part of the complex time-domain kernel $\chi_n(t) = \mathrm{Re}\, \underline{\chi}_n(t)$.

3. Formulation of the algorithm

Assuming linear, isotropic properties of the media, the dynamics of electromagnetic field in the analyzed problem is described by the second order integro-differential equation [6]

$$\nabla \times \frac{1}{\mu_0 \mu_r} \nabla \times \mathbf{E} + \sigma \frac{\partial \mathbf{E}}{\partial t} + \frac{\partial^2}{\partial t^2}\left(\varepsilon_0 \varepsilon_\infty \mathbf{E} + \sum_{n=1}^{N} \varepsilon_0 \chi_n(t) * \mathbf{E}\right) = 0, \tag{5}$$

where $\mathbf{E}$ is the time-dependent vector of the electric field intensity, $\mathbf{E} = \mathbf{E}(x, y, z, t)$. Equation (5) is an extended form of the common wave equation. It covers some problems where permittivity of materials is frequency-dependent and some broadband, non-harmonic waves propagate in the investigated case. According to the Equation (5), the distribution of the electric field depends on some traces of electromagnetic phenomena expressed by the convolution integrals $\chi_n(t) * \mathbf{E}$. They represent the frequency-dependent components of the polarization vector $\underline{\mathbf{P}}_n(\omega) = \varepsilon_0 \underline{\chi}_n(\omega)\underline{\mathbf{E}}(\omega)$.

The stated boundary value problem is solved using the Galerkin method. The discussed formulation of the finite element algorithm is based on first order Whitney elements [10]. The vector basis functions $\mathbf{w}_g$ are connected with the edges of the mesh, and belong to the space

$$W = H(\nabla\times, \Omega) = \left\{\mathbf{w}_g : \mathbf{w}_g \in L^2(\Omega), \nabla \times \mathbf{w}_g \in L^2(\Omega)\right\},$$

where L^2 is a functional space of double-summable functions [1, 10]. The created FE mesh consists of tetrahedral elements. It is inscribed into the volume of the model Ω_e using some techniques of *h*-adaptation.

The final outcome of the assembling is the ordinary differential matrix equation

$$\mathbf{Q}_\infty \cdot \frac{d^2\mathbf{e}}{dt^2} + \mathbf{Q}_0 \cdot \sum_{n=1}^{N} \frac{d^2\mathbf{c}_n}{dt^2} + \mathbf{R}_\sigma \cdot \frac{d\mathbf{e}}{dt} + \mathbf{R}_{d\Omega} \cdot \frac{d\mathbf{e}}{dt} + \mathbf{S} \cdot \mathbf{e} = \mathbf{f}, \tag{6}$$

which is coupled with a set of convolution equations

$$\underline{\mathbf{c}}_n(t) = \int_0^t \underline{\chi}_n(t-\kappa)\mathbf{e}(\kappa)d\kappa. \tag{7}$$

The vectors **e** and $\mathbf{c}_n$ gather the values of, respectively, the electric field intensity and the components of polarization along the edges of the FE mesh. The independent sources of the electromagnetic field in the model are specified in the vector **f**. The components of the matrices are expressed as either dot or vector product of the vector basis functions

$$q_{\infty,g,h} = \int_{\Omega_e} \varepsilon_0 \varepsilon_\infty \mathbf{w}_g \cdot \mathbf{w}_h d\Omega, \tag{8}$$

$$r_{g,h} = \int_{\Omega_e} \sigma \mathbf{w}_g \cdot \mathbf{w}_h d\Omega + \int_{\Gamma_e} \frac{1}{\mu c} \mathbf{w}_g \cdot (\mathbf{w}_h \times \mathbf{n}) d\Gamma, \tag{9}$$

$$s_{g,h} = \int_{\Omega_e} \frac{1}{\mu} (\nabla \times \mathbf{w}_g)(\nabla \times \mathbf{w}_h) d\Omega, \tag{10}$$

where g and h are the indexes of the edges in the model $(g,h = 1,2,\ldots N_{DOF})$, Γ is the boundary surface of the volume with the inscribed absorbing boundary conditions, and c is the speed of electromagnetic wave. The $\mathbf{Q}_0$ matrix is only defined within the regions where any dispersive material exists (i.e. $\Delta_{\varepsilon,n} > 0$), therefore its size depends on geometry and material properties of the dispersive body. The components of this matrix are given by the formula

$$q_{0,g,h} = \int_{\Omega_e} \varepsilon_0 \mathbf{w}_g \cdot \mathbf{w}_h d\Omega. \tag{11}$$

The accuracy and stability of the constructed algorithm can be controlled by the value of the time step Δ_t and applied time-integration numerical scheme. The size of the time step Δ_t remains the essential constraint of the wideband scheme. Its value arises directly from the dynamics of sources of electromagnetic field, and properties of the dispersive materials (i.e. time constants in the analyzed susceptibility submodel)

$$\Delta_t << \min\left\{\frac{1}{f_{I,u}}, \frac{2\pi}{\nu_n}, \frac{2\pi}{\sqrt{\omega_{0,n}^2 - \nu_n^2}}\right\}, \tag{12}$$

where $f_{I,u}$ is the upper frequency of the spectrum of excitation. In this approach, a single-step form of the Newmark algorithm is used [13, 14]. The field intensity and its time-derivative at the discrete time-instances $t = k\Delta_t$ ($k = 1, \ldots, N_t$) are expressed by equations

$$\mathbf{e}_{k+1} = \mathbf{e}_k + \Delta_t \dot{\mathbf{e}}_k + \frac{\Delta_t^2}{2} \ddot{\mathbf{e}}_k + \beta \Delta_t^2 (\ddot{\mathbf{e}}_{k+1} - \ddot{\mathbf{e}}_k), \tag{13}$$

$$\dot{\mathbf{e}}_{k+1} = \dot{\mathbf{e}}_k + \Delta_t \ddot{\mathbf{e}}_k + \gamma \Delta_t \left(\ddot{\mathbf{e}}_{k+1} - \ddot{\mathbf{e}}_k \right). \tag{14}$$

The algorithmic dissipation of this algorithm and its ability to damp some modes are set by the selection of β and γ coefficients.

Passing over detailed transformation, the final form of the proposed algorithm is composed of four subsequent and partially dependent phases at each time-step.

1. Phase of assembling the effective vector of excitation

$$\mathbf{b}_{k+1} = \beta \Delta_t^2 \mathbf{f}_{k+1} + \mathbf{b}_{k+1}^{\mathbf{e}} + \mathbf{b}_{k+1}^{\mathbf{e-c}} + \mathbf{b}_{k+1}^{\mathbf{c}}, \tag{15}$$

where the indicated subvectors are stated by equations

$$\mathbf{b}_{k+1}^{\mathbf{e}} = \mathbf{B}_1 \cdot \mathbf{e}_k + \mathbf{B}_{\dot{\mathbf{e}}} \cdot \dot{\mathbf{e}}_k + \mathbf{B}_{\ddot{\mathbf{e}}} \cdot \ddot{\mathbf{e}}_k, \tag{16}$$

$$\mathbf{b}_{k+1}^{\mathbf{e-c}} = \sum_{n=1}^{N} \mathbf{B}_{2,n} \cdot \mathbf{e}_k + \sum_{n=1}^{N} \mathbf{B}_{3,n} \cdot \mathbf{e}_{k-1}, \tag{17}$$

$$\mathbf{b}_{k+1}^{\mathbf{c}} = \sum_{n=1}^{N} \mathbf{C}_{1,n} \cdot \mathrm{Re}\left(\left(1 - e^{\left(-\nu_n + j\sqrt{\omega_{0,n}^2 - \nu_n^2} \right) \Delta_t} \right) \underline{\mathbf{c}}_{n,k} \right) + \sum_{n=1}^{N} \mathbf{C}_{\dot{\mathbf{c}},n} \cdot \mathrm{Re}\left(\underline{\dot{\mathbf{c}}}_{n,k} \right) + \sum_{n=1}^{N} \mathbf{C}_{\ddot{\mathbf{c}},n} \cdot \mathrm{Re}\left(\underline{\ddot{\mathbf{c}}}_{n,k} \right). \tag{18}$$

The $\mathbf{b}_{k+1}^{\mathbf{e}}$ vector gathers the strictly narrowband components, while $\mathbf{b}_{k+1}^{\mathbf{c}}$ arises due to the dispersive prosperities of materials. The $\mathbf{b}_{k+1}^{\mathbf{e-c}}$ vector emerges from recursive computation of the convolution integrals. Some quantities related to the narrowband and dispersive parts are coupled with this vector. The resulting matrices are given as

$$\mathbf{B}_1 = \mathbf{Q}_\infty + \gamma \Delta_t \mathbf{R}, \tag{19}$$

$$\mathbf{B}_{\dot{\mathbf{e}}} = \Delta_t \mathbf{Q}_\infty + (\gamma - \beta) \Delta_t^2 \mathbf{R}, \tag{20}$$

$$\mathbf{B}_{\ddot{\mathbf{e}}} = \Delta_t^2 (0{,}5 - \beta) \mathbf{Q}_\infty + 0{,}5 \Delta_t^3 (\gamma - 2\beta) \mathbf{R}, \tag{21}$$

$$\mathbf{B}_{2,n} = -\mathrm{Re}\left(\underline{v}_{n,2} \right) \mathbf{Q}_0, \tag{22}$$

$$\mathbf{B}_{3,n} = -\mathrm{Re}\left(\underline{v}_{n,3} \right) \mathbf{Q}_0, \tag{23}$$

$$\mathbf{C}_{1,n} = -\mathbf{Q}_0, \tag{24}$$

$$\mathbf{C}_{\dot{\mathbf{c}},n} = -\Delta_t \mathbf{Q}_0, \tag{25}$$

$$\mathbf{C}_{\ddot{\mathbf{c}},n} = -0{,}5 \Delta_t^2 (1 - 2\beta) \mathbf{Q}_0. \tag{26}$$

The coefficients $\underline{v}_{n,2}$, $\underline{v}_{n,3}$ and $\underline{v}_{n,1}$ in Equation (28) are gathered in the $\underline{\mathbf{v}}_n$ vector, $\underline{\mathbf{v}}_n = [\underline{v}_{n,1}\ \underline{v}_{n,2}\ \underline{v}_{n,3}]$. Their values relate directly to properties of the n-th submodel of susceptibility (cf. Eq. 36).

2. Phase of solving the linear matrix equation

$$\mathbf{A} \cdot \mathbf{e}_{k+1} = \mathbf{b}_{k+1}, \tag{27}$$

where the effective stiffness matrix is given by

$$\mathbf{A} = \mathbf{Q}_{\infty} + \gamma \Delta_t \mathbf{R} + \beta \Delta_t^2 \mathbf{S} + \sum_{n=1}^{N} \mathrm{Re}\left(\underline{v}_{n,1}\right) \mathbf{Q}_0. \tag{28}$$

3. Phase of modifying the current instances of derivatives of the field distribution. The final equations can alternatively be written as a dot product of two vectors

$$\dot{\mathbf{e}}_{k+1} = \mathbf{d}_1 \cdot \left[\mathbf{e}_{k+1} \;\; \mathbf{e}_k \;\; \dot{\mathbf{e}}_k \;\; \ddot{\mathbf{e}}_k\right], \tag{29}$$

$$\ddot{\mathbf{e}}_{k+1} = \mathbf{d}_2 \cdot \left[\mathbf{e}_{k+1} \;\; \mathbf{e}_k \;\; \dot{\mathbf{e}}_k \;\; \ddot{\mathbf{e}}_k\right]. \tag{30}$$

4. Phase of calculating temporary distributions of polarization vector and their derivatives. A general form of the recursive formula is expressed by equation

$$\underline{\mathbf{c}}_{n,k+1} = \underline{\mathbf{c}}_{n,k} \exp\left(-\left(\nu_n - j\sqrt{\omega_{0,n}^2 - \nu_n^2}\right)\Delta_t\right) + \underline{\mathbf{v}}_n \cdot \left[\mathbf{e}_{k+1} \;\; \mathbf{e}_k \;\; \mathbf{e}_{k-1}\right], \tag{31}$$

while the derivatives are expressed by the equations

$$\dot{\underline{\mathbf{c}}}_{n,k+1} = \mathbf{d}_1 \cdot \left[\underline{\mathbf{c}}_{n,k+1} \;\; \underline{\mathbf{c}}_{n,k} \;\; \dot{\underline{\mathbf{c}}}_{n,k} \;\; \ddot{\underline{\mathbf{c}}}_{n,k}\right], \tag{32}$$

$$\ddot{\underline{\mathbf{c}}}_{n,k+1} = \mathbf{d}_2 \cdot \left[\underline{\mathbf{c}}_{n,k+1} \;\; \underline{\mathbf{c}}_{n,k} \;\; \dot{\underline{\mathbf{c}}}_{n,k} \;\; \ddot{\underline{\mathbf{c}}}_{n,k}\right]. \tag{33}$$

The number of convolution Equations (31) and vector Equations (32)-(33) processed in the fourth phase is equivalent to the number of submodels of susceptibility (2).

The flow-chart of this scheme is depicted in Figure 1. The solid lines define relations for the strictly single-step scheme, while the dashed lines indicate some paths for the two-step algorithm. According to the definition of $\mathbf{B}_{3,n}$ matrix, the single-step form of the constructed wideband algorithm is only assured when the $\underline{v}_{n,3}$ component is equal to zero.

The representation of the processed field variables allows for casting two coupled sections in the algorithm. Real temporary distributions of electric field and their derivatives are computed in phases 1, 2, and 3. Since the exponential form of susceptibility is used, the equations assigned to the fourth phase are complex-valued. The selection of the real part is a function lock between the narrowband and the convolution parts of the algorithm.

The structure and properties of the proposed wideband FE algorithm can be modified in the narrowband and convolution phases. Following the properties of the Newmark algorithm, the selection of β and γ coefficients enable one to obtain a set of second order time-integration schemes.

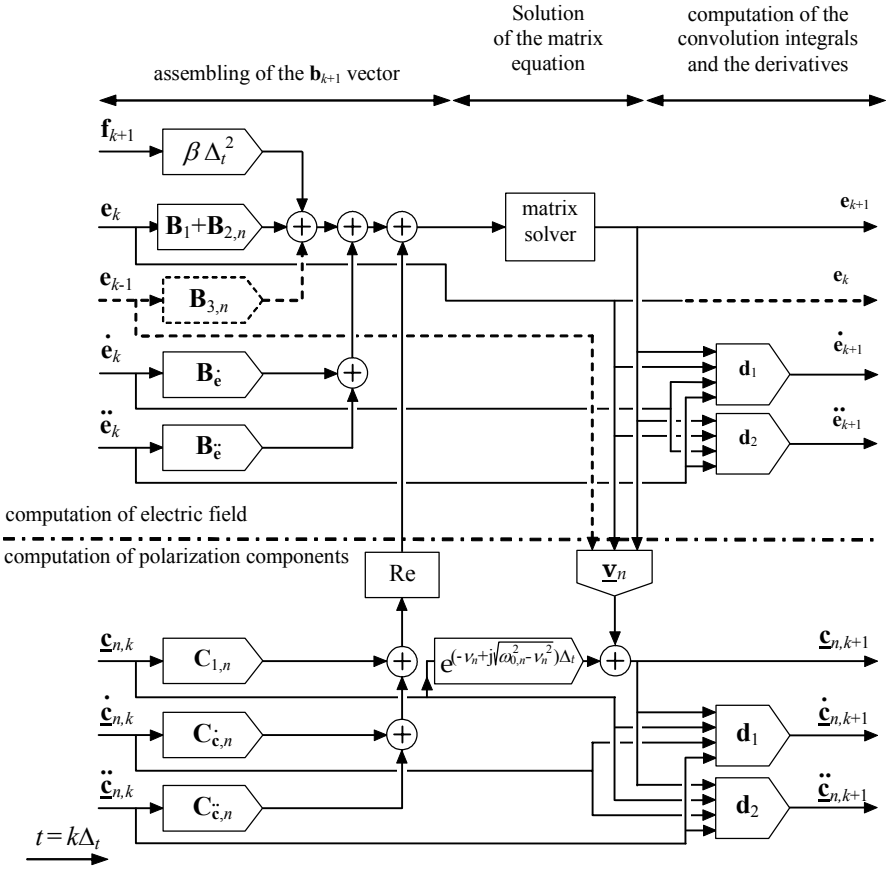

Fig. 1. Relations between data and tasks within the single-step wideband FETD algorithm

The vectors $\mathbf{d}_1$ and $\mathbf{d}_2$, which are indispensable in the second and fourth phases, remain constant during the simulation, and their components depend on the assumed parameters of the Newmark scheme

$$\mathbf{d}_1 = \frac{1}{2\beta\Delta_t}\left[2\gamma \quad -2\gamma \quad 2\Delta_t(\beta-\gamma) \quad \Delta_t^2(2\beta-\gamma)\right], \tag{34}$$

$$\mathbf{d}_2 = \frac{1}{2\beta\Delta_t^2}\left[2 \quad -2 \quad -2\Delta_t \quad \Delta_t^2(2\beta-1)\right]. \tag{35}$$

Electromagnetic energy in the model is conserved, and the scheme remains unconditionally stable when $\beta = 0{,}25$ and $\gamma = 0{,}5$ [9].

The second method of modification of the algorithm is hidden in the form of the $\underline{\mathbf{v}}_n$ vector. Its components appear in Eqs. (17), (28) and (31). Their values depend on the assumed method of approximation of electrical field distribution in an elementary period $t \in \langle k\Delta_t, (k+1)\Delta_t \rangle$.

The formulated algorithm enables one to implement some different schemes of approximation. The presented formulation is limited to the two-step scheme of approximation, and the simplest one is the constant recursive algorithm, $\mathbf{e}_{k+1} = \mathbf{e}_k$. In that case the vector of coefficients can be expressed as

$$\underline{\mathbf{y}}_n = -j \frac{\Delta_{\varepsilon,n}\omega_{0,n}^2}{\sqrt{\omega_{0,n}^2 - \nu_n^2}} \frac{1 - \exp\left(-\left(\nu_n - j\sqrt{\omega_{0,n}^2 - \nu_n^2}\right)\Delta_t\right)}{\nu_n - j\sqrt{\omega_{0,n}^2 - \nu_n^2}} [0\ 1\ 0]. \tag{36}$$

Considering a higher-order scheme, the final form of the vector would not change, but the mathematical expression would be more complex. Consequently, the computational cost of the FE algorithm would increase. The given scheme of approximation can be independently matched to each n-th submodel of susceptibility.

4. Validation of the algorithm

The properties of the algorithm were examined using a benchmark model. In the presented case study, an incident electromagnetic pulse propagates through the space and interacts with a frequency-selective body placed in the center of the analyzed volume. The configuration of the problem is shown in Figure 2. The unbounded domain of the problem is reduced to a cube ($x_\Omega = y_\Omega = z_\Omega = 50$ mm). The first-order Engquist-Majda boundary condition is implemented on the external surface of the model [1].

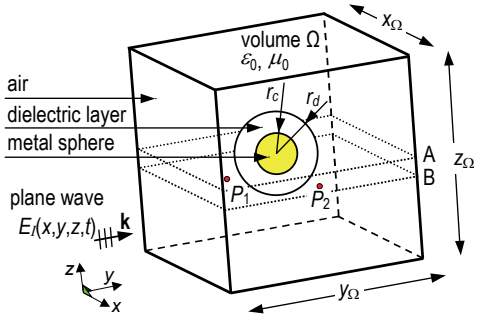

Fig. 2. Geometry of the discussed benchmark problem with a conducting sphere covered by a dispersive layer ($r_c = 5$ mm; $r_d = 10$ mm)

The affected object consists of a dielectric, dispersive layer placed on a perfectly conducting sphere. This layer changes the dynamics of the electromagnetic response and the equivalent radar cross-section of the analyzed object. The narrowband, selective nature of the dielectric sheath is expressed by a linear combination of the three resonance submodels (2). The constitutive parameters of the submodels are shown in Table 1.

Table 1. Material constants assumed in the third-order resonance model of permittivity of the dielectric layer

ε_∞	Components of susceptibility			
	n	$\Delta_{\varepsilon,n}$	$\omega_{0,n}$ [rd/s]	ν_n [rd/s]
4	1	0.333	$1\cdot10^9$	$3.333\cdot10^8$
	2	0.333	$5\cdot10^9$	$1.667\cdot10^9$
	3	0.333	$2.5\cdot10^{10}$	$8.333\cdot10^9$

The plots of the real and imaginary components of permittivity

$$\varepsilon_r'(\omega) = \mathrm{Re}\,\underline{\varepsilon}_r(\omega) = \varepsilon_\infty + \sum_{n=1}^{N} \frac{\Delta_{\varepsilon,n}\omega_{0,n}^2\left(\omega_{0,n}^2 - \omega^2\right)}{\left(\omega_{0,n}^2 - \omega^2\right)^2 + (2\omega\nu_n)^2}, \tag{37}$$

$$\varepsilon_r''(\omega) = \mathrm{Im}\,\underline{\varepsilon}_r(\omega) = \sum_{n=1}^{N} \frac{\Delta_{\varepsilon,n}\omega_{0,n}^2 2\omega\nu_n}{\left(\omega_{0,n}^2 - \omega^2\right)^2 + (2\omega\nu_n)^2}, \tag{38}$$

as a function of frequency are presented in Figure 3.

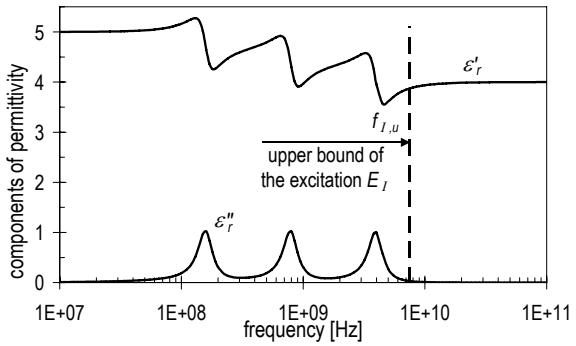

Fig. 3. Real and imaginary parts of permittivity for the assumed dispersive dielectric

The assumed body is illuminated by a plane wave $\{E_z, H_x\}$. It propagates along the y axis ($\mathbf{k} = \mathbf{1}_y$), and the time signature of the wave is a Gaussian function

$$\mathbf{E}_I(0,t) = E_{z,\max}\exp\left(-\alpha_I^2(t-t_I)^2\right)\mathbf{1}_z\,\mathbf{1}(t), \tag{39}$$

where α_I and t_I are respectively the decrement and the time shift of the impulse. These parameters of the excitation wave are equal, respectively, to $4\cdot10^{10}$ s^{-1} and $7.5\cdot10^{-11}$ s. In that case the spectrum of the impulse reaches the frequency of over $f_{I,u}$ = 7.5 GHz (Fig. 3).

To get a quantitative estimate of the field behaviors, the computed values are registered on selected horizontal cross-sections of the model (denoted as A and B in Fig. 2). The example snapshots of the computed electric field distribution are presented in Figure 4.

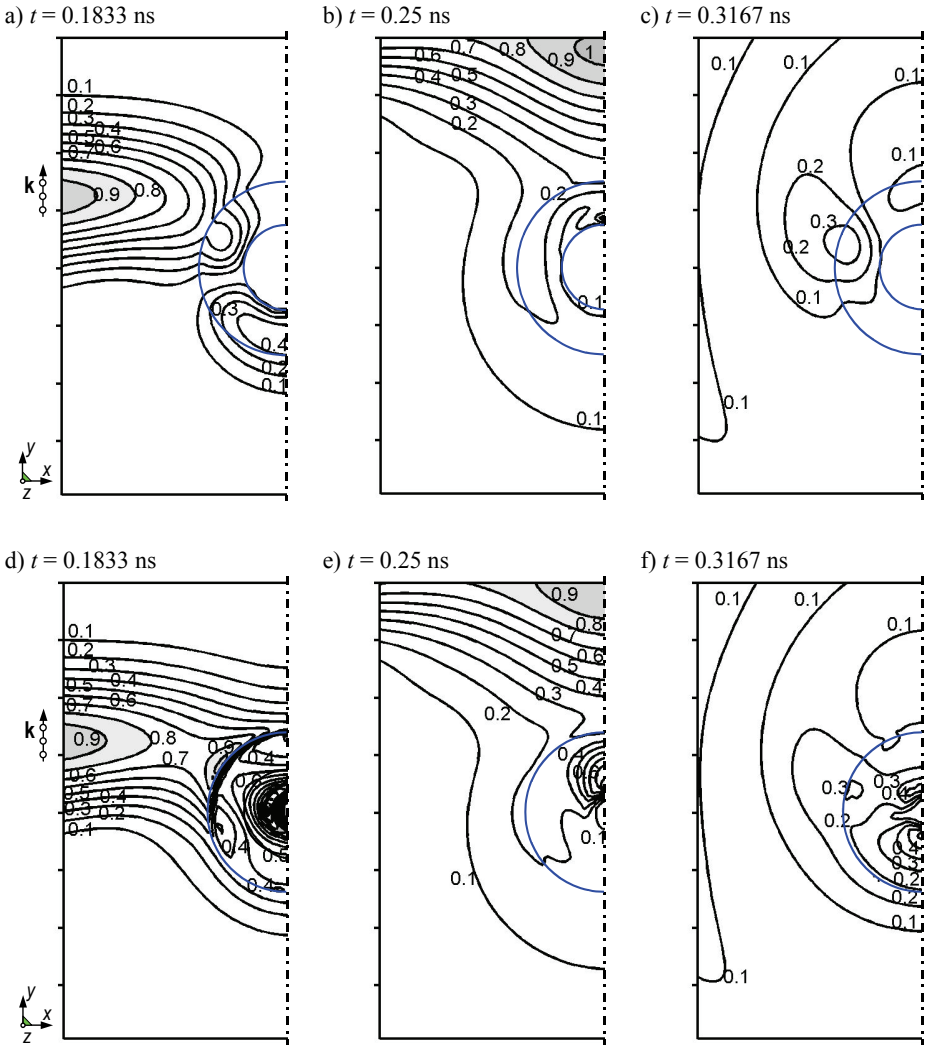

Fig. 4. Distribution of electric field intensity at different time steps, registered on surfaces A (upper figures) and B (lower figures)

The variation of relative modulus of electric field intensity is plotted in Figure 5. For the sake of comparison, the results obtained from the finite difference time-domain algorithm (FDTD) are presented in the same figure. The constructed FD model with the regular, cubical Yee mesh is calculated using the Meep package [11]. Its broadband implementation is based on the recursive convolution technique [15]. Good correspondence between both algorithms is evident from the figures.

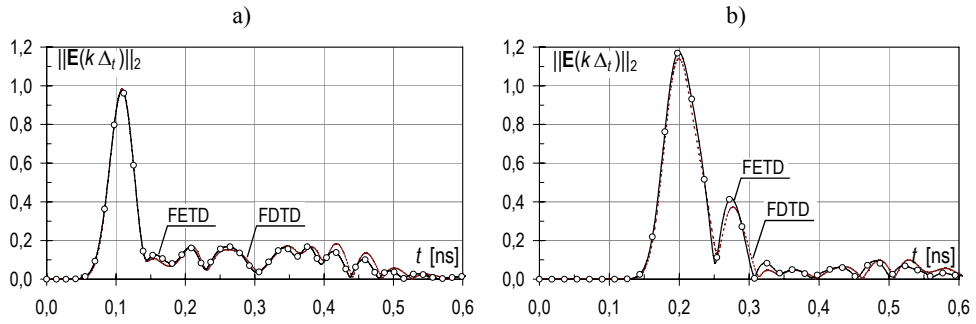

Fig. 5. Relative modulus of the electric field intensity registered in the points depicted in Fig. 2: $P_1(25, 10, 20)$ [mm], $P_2(25, 34, 15)$ [mm]

5. Conclusions

The presented single-step, broadband algorithm enables one to analyze the problems with some frequency-selective linear materials. The essential point in the construction of the flexible finite element scheme is functional relations between the strictly narrowband and the convolution parts. In the constructed scheme, the dependencies between these tasks can be shaped independently for each submodel of susceptibility.

Due to the single-step form of the time-integration scheme and the convolution subroutine, the FE mesh can be adapted and modified during computations. Since the law of conservation of energy must be fulfilled, the mesh can be modified in the nondispersive regions. The FE elements inscribed in the dispersive regions should remain unchanged, because the values of the convolution integrals collect the information about previous, local distributions of the field in the selected region.

The complex form of the numerical scheme has an effect on the final computational costs of the algorithm. The comparative analysis indicates larger memory cost of the single-step algorithm than the commonly used two-step finite element scheme [2, 4, 9]. In the worst case, when dispersive material occupies the whole volume of the model, the memory cost of the single-step scheme is at least 24% higher than that of the two-step one.

The discussed finite element algorithm can be efficiently implemented in problems with highly non-homogeneous material structure. The size and construction of the FE mesh can be adapted to properties of materials. The commonly used FDTD algorithms require the uniform hexahedral mesh. Therefore, the size of the FDTD model can be larger, but the total time of computations and the performance of this algorithm remain better than the FE one [3]. The FDTD algorithm remains explicit in the wideband formulation. The solution of matrix Equation (27) is the most time-consuming part of the presented implicit finite element scheme.

References

[1] Butryło B., Vollaire C., Nicolas L., *Stability and fidelity of the finite element time domain method with distorted mesh*. IEEE Transactions on Magnetics 40(2): 1424-1427 (2004).

[2] Butryło B., *High frequency electric relaxation of materials and its impact on distribution of electromagnetic field in dispersive dielectric placed on the conducting bodies* (in Polish). Przegląd Elektrotechniczny 86(4): 111-114 (2010).
[3] Butryło B., Vollaire C., Nicolas L., *Parallel implementation of the vector finite element and finite difference time domain methods*. Parelec: International Conference on Parallel Computing in Electrical Engineering, IEEE Computer Society, pp. 347-352 (2002).
[4] Edelvik F., Strand B., *Frequency dispersive materials for 3-D hybrid solvers in time domain*. IEEE Transactions on Antennas and Propagation 51(6): 1199-1205 (2003).
[5] Koledintseva M.Y., Drewniak J.L., Pommerenke D.J. et al., *Wide-band Lorentzian media in the FDTD algorithm*. IEEE Transactions on Electromagnetic Compatibility 47(2): 392-399 (2005).
[6] Kristensson G., Karlson A., Rikte S., *Electromagnetic wave propagation in dispersive and complex material with time domain techniques*. Lund Institute of Technology, report Coden:Lutedx/(TEAT-7086)/1-38 (2001).
[7] Kyriazidou C.A., Diaz R E., Alexopoulos N.G., *Novel material with narrow-band transparency window in the bulk*. IEEE Transactions on Antennas and Propagation 48(1): 107-116 (2000).
[8] Li J., *Error analysis of fully discrete mixed finite element schemes for 3-D Maxwell's equations in dispersive media*. Computer Methods in Applied Mechanics and Engineering 196: 3081-3094 (2007).
[9] Maradei F., *A frequency-dependent WETD formulation for dispersive materials*. IEEE Transactions on Magnetics, 37(5): 3303-3306 (2001).
[10] Monk P., *Finite element methods for Maxwell's equations*. Oxford University Press, Oxford (2003).
[11] Oskooi A.F., Roundy D., Ibanescu M., Bermel P., Joannopoulos J.D., Johnson S.G., *Meep: A flexible free-software package for electromagnetic simulations by the FDTD method*. Computer Physics Communications 181: 687–702 (2010).
[12] Silveirinha M.G., Fernandes C.A., Costa J.R., *Electromagnetic characterization of textured surfaces formed by metallic pins*. IEEE Transactions on Antennas and Propagation 56(2): 405-416 (2008).
[13] Van T., Wood A., *A time-domain finite element method for Maxwell's equations*. SIAM Journal on Numerical Analysis 42(4): 1592-1609 (2004).
[14] Wood W.L., *Practical time-stepping schemes*. Clarendon Press, Oxford (1990).
[15] Young J.L., Nelson R.O., *A summary and systematic analysis of FDTD algorithms for linearly dispersive media*. IEEE Antennas and Propagation Magazine: 43(1): 61-77 (2001).
[16] Zhou Z., Melde K.L., *A comprehensive technique to determine the broadband physically consistent material characteristics of microstrip lines*. IEEE Transactions on Microwave Theory and Techniques 58(1): 185-194 (2010).